A multiscale description of charge transport in conjugated oligomers

Victor Rühle,[1,a)] James Kirkpatrick,[2,b)] and Denis Andrienko[1,c)]
[1]*Max Planck Institute for Polymer Research, Ackermannweg 10, Mainz 55128, Germany*
[2]*Department of Physics, Imperial College London, Prince Consort Road, London SW7 2BW, United Kingdom*

(Received 11 December 2009; accepted 10 February 2010; published online 2 April 2010)

By relating inter- and intrachain ordering to charge dynamics a correlation between the morphology and charge mobility of neutral and doped states of a conjugated polymer, in this case polypyrrole, is established. Morphologies are generated using an all-atom force field, while charge dynamics is simulated within the framework of high temperature nonadiabatic Marcus theory. For short oligomers, charge carrier mobility is insensitive to the orientational molecular ordering and is determined by the threshold transfer integral which connects percolating clusters of molecules, forming interconnected networks. The value of this transfer integral can be estimated from the radial distribution function. We therefore find that charge mobility is mainly determined by the local molecular packing and is independent of global morphology, at least in such a noncrystalline state of a polymer. © *2010 American Institute of Physics*. [doi:10.1063/1.3352568]

I. INTRODUCTION

Organic electronics promises the possibility of developing devices with the electronic properties of inorganic materials and the advantageous processing properties of plastic materials. At present, four distinct classes of organic conductive materials are being scrutinized for organic electronics applications. (i) Small organic molecules assembled in crystals, normally by a vapor deposition. Typical examples here are polyacene or rubrene crystals.[1,2] (ii) Soluble small organic molecules which self-assemble in supramolecular structures (molecular wires). Discotic liquid crystals and some organic oligomers are typical representatives of such materials.[3–5] (iii) Soluble conjugated polymers, such as derivatives of polythiophene, poly(p-phenylene vinylene).[6,7] (iv) Finally, doped conjugated polymers such as polyacetylene and polypyrrole (PPy).[8–10]

For the majority of applications two requirements are essential: high charge carrier mobilities and stability of materials. The advantage of organic materials is that synthesis can be used to tune molecular properties. Indeed, significant efforts have been invested in improvement of charge mobilities and success has been reported.[11,12] It has been concluded, however, that optimizing the electronic structure is not sufficient, since the material morphology, which heavily depends on a processing technique, can alter charge mobility by orders of magnitude.[13,14] Because of this, the formulation of comprehensive structure-property relationships has been so far very difficult. In this situation, computer simulations could help to more accurately characterize the material morphology, to disentangle contributions of the electronic structure and morphology and, eventually, help to rationally design organic semiconductors.[15,16]

In this paper, a computational study of the relationship between the arrangement of polymer chains and charge mobility is presented for neutral and oxidized oligomers of PPy. PPy is known to have good conducting properties when oxidized,[17] with conductivities up to 300 S cm^{-1}. Similar to the other conjugated polymers, insolubility of PPy in organic solvents hinders detailed structural analysis. Therefore, much about the physical properties and structural characteristics is not understood and reports are often contradictory.[18] An experimental overview of electrochemistry of conducting PPy films is given in Ref. 19.

The model we use is based on our previous work on charge transport in discotic liquid crystals.[20–27] We first explicitly simulate the morphology of an assembly of chains using molecular dynamics (MD). In order to tweak the morphology two methods are used: the initial arrangement of polymer backbones for the MD simulation is changed and the simulation is performed on oxidized polymer chains in the presence of counterions. In particular we use three types of chain alignment: all the chains aligned in one direction, the chains lying in one plane, and an isotropic arrangement of chains. The morphology is then used to compute charge transfer rates and hence charge mobility. The main change in the modeling of charge transport is that we define charge transfer units in terms of subsets of the polymer chain (conjugated segments), use different rates for intra- and intermolecular transport, and compute the nearest neighbor list for the three dimensional network of chains.

In discotic liquid crystals we argued that the distribution of the intermolecular transfer integrals, which is directly linked to the azimuthal register and separation between the molecules, determines the value of charge mobility. The charge transport in these systems has one dimensional character and is limited by the tail of small transfer integrals (defects) in the system. This can easily be rationalized because in one dimension the smallest transfer integrals will be bottlenecks for charge transfer. The assembly of PPy that we study is of course not one dimensional and therefore it is

[a)]Electronic mail: ruehle@mpip-mainz.mpg.de.
[b)]Electronic mail: james.kirkpatrick@imperial.ac.uk.
[c)]Electronic mail: denis.andrienko@mpip-mainz.mpg.de.

harder to predict what the bottleneck of charge transport is. We argue that charge mobility in this case is almost entirely determined by the magnitude of the transfer integral which allows the whole simulation box to be connected together. Most intriguingly, the size of this transfer integral is not strongly affected by the changes in morphology we have imposed. Therefore our main conclusion is that for the case of such amorphous polymers, charge mobility is mostly determined by local packing and is almost independent on the alignment of chains.

II. MORPHOLOGIES

In order to generate large-scale morphologies at an atomistic level of detail one first needs to develop a reliable force field for PPy oligomers. Some work in this direction has already been undertaken by Cascales *et al.*[28,29] who analyzed swelling of PPy upon oxidation as well as diffusion of chloride counterions in the PPy network. We have refined the force-field parameters by using the available bonded and nonbonded parameters from the OPLS-AA force field of a pyrrole monomer.[30] The parameters of the dihedral and the improper connecting the neighboring monomers were obtained by fitting the potential energy surface to first principles calculations. For a neutral PPy the procedure is described in detail in Ref. 31. A similar strategy was used to derive the force field for oxidized PPy. It is described in detail in Appendix, Sec. 1.

With the force field at hand, we prepared three kinds of molecular morphologies, with a different degree of molecular ordering, which we will refer to as *fiber*, *slice*, and *isotropic*. In case of the fiber, polymer chains (originally set up on an ideal lattice with experimental density for liquid pyrrole) were aligned along the x axis and shuffled randomly in the unit cell. The slice morphology was generated by randomly rotating chains in the xz plane, as well as along the chain axis and again shuffled randomly. Finally, isotropic configuration was achieved by assigning random orientations to all the chains and randomly translating them in space. Using liquid crystalline terminology, fiber corresponds to a nematic mesophase with the order parameter $S=1$, slice with $S=-1/2$, and isotropic morphology to the isotropic mesophase with $S=0$.

All systems consisted of 10 repeat unit oligomers, 512 (256 for the fiber) molecules in total. To remove overlaps between chains, we performed a short run slowly switching on nonbonded interactions. To locally equilibrate the systems, the conformations were then heated up to 500 K for 5 ns. Finally the systems were cooled down to 300 K during 1 ns followed by a final equilibration at room temperature for 2 ns. All runs were performed using the GROMACS package.[32] For the charge transport calculations, 50 snapshots were saved every 2 ps. Representative snapshots of all three morphologies are shown in Fig. 1.

In the oxidized case, we assumed three charges per chain[33] and used three Cl^- as counterions. A conformation from the neutral equilibration run was taken as a starting point. Charges and the dihedral parameter of the force field were changed to the oxidized ones and counterions added at random positions. The nonbonded interactions of the counterions were slowly switched on during a stochastic dynamics run.

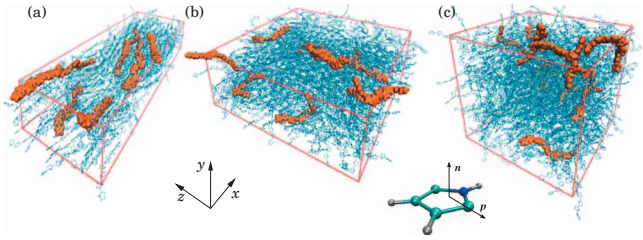

FIG. 1. Representative snapshots of three different molecular arrangements. (a) Fiber with all molecules aligned along the z axis. (b) Slice with all molecules aligned in the xy plane. (c) Isotropic with randomly oriented molecules. To emphasize molecular alignment, several randomly chosen molecules are shown using a different representation.

To characterize the generated morphologies, we calculate the radial distribution function of the centers of mass of the repeat units, as well as two order parameters, based on vectors $\boldsymbol{n}$ normal to the pyrrole repeat unit planes and vector $\boldsymbol{p}$ along atoms where adjacent units are attached to (see the inset in Fig. 1). The order parameter is defined as the largest eigenvalue of the nematic order tensor

$$S_{\alpha\beta} = \frac{1}{2}\langle 3u_\alpha u_\beta - \delta_{\alpha\beta}\rangle, \tag{1}$$

where $\alpha,\beta=x,y,z$, $\boldsymbol{u}$ is a unit vector of interest, and $\langle\cdots\rangle$ denotes time and ensemble average.

III. CHARGE CARRIER MOBILITIES

The main issue in order to simulate charge dynamics is to determine the charge transport unit. Many possible phenomena can localize charges on a polymer: polaron self-trapping,[34,35] breaks in conjugation due to chemical defects[36] or due to the torsion angle between neighboring monomers,[37] and finally rapidly changing intramolecular transfer integrals affecting the dynamic disorder which is responsible for charge localization in molecular crystals.[38,39]

Three limiting cases for charge localization can be addressed by our code: a totally localized model where each repeat unit is a charge transporting unit, a totally delocalized model where each oligomer is a charge transporting unit, and finally a model where the polymer is cut into segments. The places where the oligomer is artificially cut are chosen when the torsion angle between two repeat units is greater than 45°. When computing mobilities we always use the model where a distribution in conjugation lengths is considered; however the totally localized model is used to investigate the effect of changing intramolecular rates and totally delocalized model is used when we want to investigate percolation of intermolecular rates while entirely excluding intramolecular transfer integrals.

Having defined the charge transport units, it remains to choose an expression for the charge hopping rates. We must distinguish between the cases of transport along chains and between chains. Since the typical internal reorganization alone is approximately 0.4 eV (depending on conjugation length) and the peak in intermolecular transfer integrals is at approximately 10 meV, it is reasonable to treat this transport

in the nonadiabatic regime. On the other hand, transport along the chain can occur with transfer integrals as large as $J_0 \cos(\pi/4) \sim 0.7$ eV. Such transfer integrals put transport firmly in the adiabatic regime and possibly even in the delocalized regime and therefore must be described by a different formula. For nonadiabatic transport we use the semiclassical Marcus theory[40,41]

$$\omega_{ij} = \frac{J_{ij}^2}{\hbar}\sqrt{\frac{\pi}{\lambda_{ij} k_B T}}\exp\left[-\frac{(\Delta E_{ij} - \lambda_{ij})^2}{4\lambda_{ij} k_B T}\right], \quad (2)$$

where k_B is Boltzmann's constant, $\hbar$ is the Planck constant, λ_{ij} is the reorganization energy, $\Delta E_{ij} = -(\epsilon_{\mathrm{HOMO}}^{(j)} - \epsilon_{\mathrm{HOMO}}^{(i)})$ is the difference in energies of the sites i and j, and J_{ij} is the corresponding transfer integral. In principle it would also be possible to compute the contribution to site energy differences from electrostatic energies. There is a significant problem in doing this in the case when the dielectric constant is not only due to electronic polarization, as it is in the case of the oxidized polymer. In the case of a heavily doped polyelectrolyte, in fact, even the optical dielectric constant can be very large—up to 20 according to some measurements.[42] Under such circumstances, decoupling the MD from the charge dynamics becomes rather contrived as rearrangement of ions would make the largest contribution to the dielectric constant. We choose instead to concentrate on the effect of conjugated segment length on site energy, in this sense we are concentrating on the *morphology* effect of charging chains and hence stiffening them.

Hence, the key parameters we need to know in order to understand charge dynamics are the transfer integral between conjugated segments, the site energy, and the reorganization energy. The reorganization energy λ_i of an oligomer of length i can be computed using the method described in Ref. 43. The reorganization energy for transfer between oligomers of different length was estimated by taking $\lambda_{ij} = \frac{1}{2}(\lambda_i + \lambda_j)$.

Intermolecular transfer integrals J_{ij} are computed by the expectation value of the Fock operator of the pair of molecules with highest occupied molecular orbitals (HOMOs) localized on each unit. The Fock matrix is computed using the INDO assumptions with Zerner's parametrization and a simplified approach which does not require computation of the density matrix of the pair of molecules, as described in Ref. 44.

For the adiabatic transport instead, we use a simple expression derived from transition state theory[40,43]

$$\tau_{ij} = \nu \exp\left[-\frac{(\Delta E_{ij} - \lambda_{ij})^2}{4\lambda_{ij} k_B T} - \frac{|J_0 \cos\theta_{ij}|}{kT}\right]. \quad (3)$$

In this equation ν is a prefactor related to the frequency of the promoting mode and the relevant Franck–Condon factor.[40] Simulations where charges are allowed to hop only between *monomers* have shown that a value of 10^{15} s^{-1} is sufficient to stop the global mobility depending on the choice of this parameter. By making sure that this rate is sufficiently fast we therefore ensure that the rate limiting step in charge transport simulations is always an intermolecular process.

Note that the intramolecular transfer integral is modeled by the following form: $J_{\mathrm{intra}} = J_0 \cos\theta_{ij}$, where θ_{ij} is the torsional angle between neighboring charge transport units i and j, and J_0 is chosen to have a value of 1 eV. All other symbols have the same meaning as in Eq. (2).

Oxidation is believed to have two main effects on charge mobility: it makes the polymer backbones significantly stiffer and it also changes the mediators of charge transport from polarons to bipolarons.[45–50] If we consider two charge transporting units that can support either polarons or bipolarons, we can imagine two ways that charges move: either two charges move at once or one moves at a time. We can distinguish which of these cases is more likely by considering the transfer integral related to each case. Using Slater rules and within the frozen orbital approximation, we deduce that in the latter case the transfer integral will correspond to the exchange integral of those two orbitals, whereas in the former case the transfer integral will correspond again to the expectation value of the Fock matrix. Since the expectation value of the Fock matrix is always greater than the exchange integral it is much faster for a single charge to be exchanged between molecules. The mobility that we compute in the case of oxidized PPy is the mobility of a single charge moving on a background of overall charged oligomers. The charge of each oligomer is deduced from its length; oligomers of length one to three will vary from having one charge to having two charges, lengths four to six vary from having two charges to three charges, and longer oligomers vary from three to four charges. The transfer integrals are computed using the relevant molecular orbitals.

Once the position of atoms is determined from MD, the oligomers are segmented into conjugated units using the condition that if the absolute value of the torsion between subsequent monomers is greater than 45°, the monomers are considered as belonging to different conjugated segments. Each oligomer has then its position and orbitals adjusted to the remaining torsions to ensure a close match to the atomistic morphology. Transfer integrals, site energies, and rates of charge transfer are then computed using the methodologies described above.

The charge dynamics is simulated using kinetic Monte Carlo algorithm.[51] The average drift velocity of charges in an electric field is averaged over several different frames from the MD to ensure good statistics. All simulations were performed using in-house developed software package VOTCA.[52]

IV. RESULTS AND DISCUSSION

In order to confirm that the three starting morphologies and the two different force fields corresponding to a flexible reduced polymer or a stiff oxidized one have indeed resulted in assemblies with different degrees of orientational ordering of chains, three order parameters were computed for each morphology: S_n, S_p, and $S_{\text{end-end}}$. The physical meaning of vectors $\boldsymbol{n}$, $\boldsymbol{p}$ is shown in Fig. 1. For $S_{\text{end-end}}$ the end-to-end vector was used.

The results are summarized in Table I. The fiber has rather large nematic order parameter $S_{\text{end-end}}$, which indicates a good alignment of the chains along the x axis. The slice has a negative value of the order parameter, which is in agreement with the (practically isotropic) molecular ordering in

TABLE I. Order parameters calculated for $\boldsymbol{n}$, $\boldsymbol{p}$, and end-to-end vectors which characterize average orientational ordering of repeat units in oligomers (S_n,S_p) and chains in a simulation box ($S_{\text{end-end}}$).

	Neutral			Oxidized		
Morphology	S_n	S_p	$S_{\text{end-end}}$	S_n	S_p	$S_{\text{end-end}}$
Fiber	−0.38	0.70	0.85	−0.38	0.64	0.84
Slice	0.36	−0.27	−0.33	0.34	−0.24	−0.30
Isotropic	−0.14	0.13	0.16	0.10	0.10	0.14

the *xz* plane. Finally, the isotropic morphology has a rather small value of the order parameter, which is again in agreement with the practically isotropic distribution of molecular orientations in the box. The same trend can be observed for the oxidized PPy morphologies, where the stiffness of chains does not really affect the orientational ordering of oligomers.

With the atomistic geometries at hand we can now calculate charge transport parameters needed to simulate charge dynamics. We consider torsional defects as the main source of charge localization in PPy, as explained in Sec. III. The concept is illustrated in the inset of Fig. 2(b).

We will start by analyzing the effect of segment length on *interchain* rates, ω_{ij}. An increase in the site energy ϵ_{HOMO} with the increase in the length of an oligomer, which is shown in Fig. 2(a), indicates that positive charges (holes) prefer to occupy larger charge transport units. A slight complication to this is the fact that the reorganization energy λ also depends on the length of oligomer considered, as shown in Fig. 2(b). With the exception of oligomers of length 1 repeat unit (ru), the reorganization energy decreases with length of a conjugated segment. The net effect on the rate, therefore, is that jumps from shorter to longer segments are in general favored, but if the length difference is too great, the rates become slow due to being in the inverted regime of Marcus theory. These observations are summarized in Fig. 2(c), which shows the rate between two oligomers as a function of their size. It is clear that the rate prefactor (excluding the transfer integral) is, relatively speaking, rather insensitive to oligomer length in a large region. Essentially, energetic disorder becomes a minor effect if oligomer lengths become greater than 3 ru.

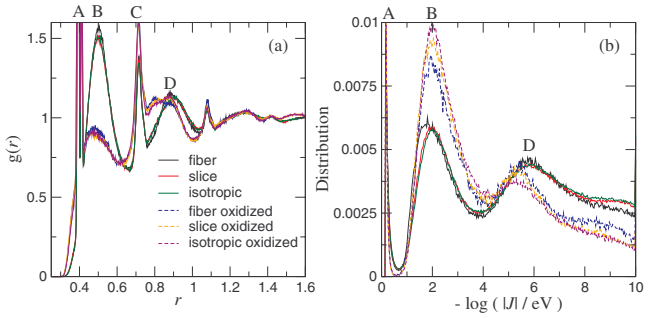

FIG. 3. Radial distribution function for monomers (a) and distribution of logarithm of transfer integrals (b) for three different morphologies and two oxidation states. The distribution of transfer integrals is normalized to the *total* number of transfer integrals in the morphology. Peak A is due to intramolecular charge transfer between neighboring repeat units, peak B is due to the intermolecular transfer for the first shell of neighbors, peak C is due to next nearest neighbors along the chain (and therefore is absent in the distribution of the transfer integrals), and peak D corresponds to the second shell of neighbors participating in the intermolecular charge transfer.

Most of the disorder introduced in the simulation is, therefore, a result of the distribution of transfer integrals, shown in Fig. 3(b). Showing the distribution of transfer integrals next to the radial distribution function, Fig. 3(a), reveals how intimately these two quantities are related. Note that this relation becomes evident only if the *logarithm* of the transfer integrals is compared with the radial distribution functions. The radial distribution function shows the density at a shell at a certain distance from the center of a monomer. The first two sharp peaks (both labeled with letter A) correspond to the nearest intrachain neighbors (there are two peaks because the two possible orientations of an intrachain neighbor result in slightly different distances). The next peak (B) corresponds to the nearest interchain neighbor. This structure is exactly repeated in the distribution of logarithms of the transfer integral.

We can also see that even though the different morphologies have very different order parameters and seem very different to the naked eye, the transfer integrals are in fact rather similar. This is because transfer integrals are essentially a local property which depends only very weakly on the global ordering. The only morphology which does

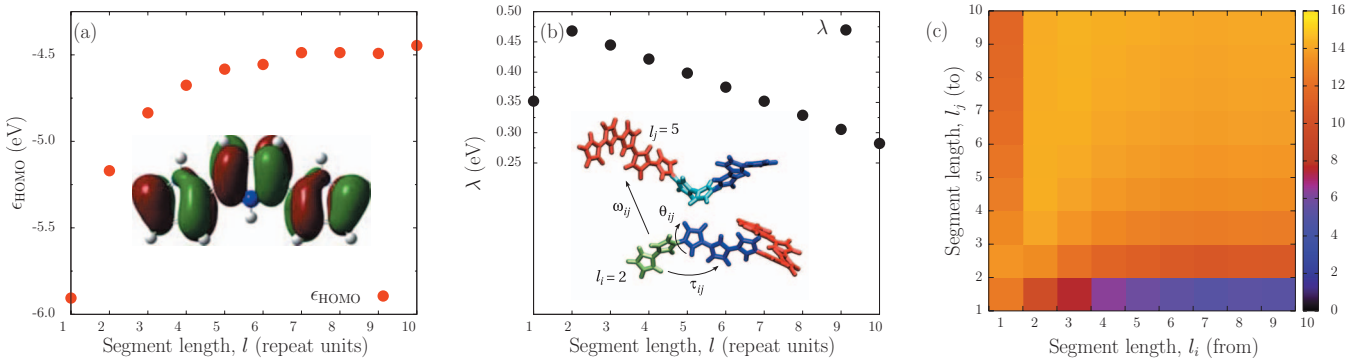

FIG. 2. (a) Dependence of the HOMO energy of the oligomer on its length. HOMO orbital of a PPy trimer is depicted in the inset. (b) Dependence of the reorganization energy λ_i on oligomer length i. The inset illustrates the concept of a conjugated segment (charge transport unit). τ_{ij} is the intrachain and ω_{ij} is the interchain transfer rate. (c) Dependence of the rate (assuming a transfer integral of 0.1 eV in units of s^{-1}) on the length of the oligomer from which the charge is hopping (x axis) and on the length of the oligomer to which it is hopping (y-axis).

TABLE II. Mobilities in different directions for various morphologies in 10^{-2} $cm^2\ V^{-1}\ s^{-1}$. Mobility was computed from 100 frames with an electric field of 10^5 $V\ m^{-1}$, considering a distribution of conjugated fragments and averaging only those values greater than 10^{-6} $cm^2\ V^{-1}\ s^{-1}$. The reason for excluding the lower mobility simulations and the frequency of those occurrences is explained in the seventh paragraph of Sec. IV.

Morphology	Mobility x	Mobility y	Mobility z
Fiber	2.3 ± 1.6	1.8 ± 1.0	1.7 ± 0.9
Slice	1.3 ± 0.4	0.7 ± 0.3	1.2 ± 0.4
Iso	0.8 ± 0.3	0.7 ± 0.2	0.9 ± 0.3
Fiber ox	1.9 ± 1.8	1.5 ± 1.1	1.1 ± 1.0
Slice ox	2.6 ± 2.1	2.4 ± 1.5	3.0 ± 2.1
Iso ox	3.5 ± 1.7	3.1 ± 1.5	3.4 ± 1.5

display a small difference in transfer integrals is the fiber morphology in the reduced form for which the peak of the transfer integrals is slightly greater. Notice that the height of the peaks in the distribution of transfer integrals is somewhat deceiving, since all distributions are normalized by the total number of neighbors. A higher first peak is likely to represent fewer second nearest neighbors within the cutoff distance rather than more nearest neighbors. This is why the oxidized geometries, with their longer average lengths, tend to have a higher first peak.

Table II shows the mobility computed on the different morphologies using kinetic Monte Carlo and averaged over 100 different frames from MD. The values were computed considering a distribution of conjugation lengths. Values were averaged only if their value was greater than 10^{-6} $cm^2\ V^{-1}\ s^{-1}$. A cutoff must be chosen because if a simulation is started with a charge on a conjugated unit of length 1 or 2 ru, it is very unlikely to escape due to being in the inverted regime, as shown in Fig. 2, on average for our simulations this happens for 7.4% of simulations. As argued in the Appendix, this is justified because torsional angles fluctuate on a time scale significantly faster than those very slow hops: in other words the charge on a short transport unit would be delocalized by vibrations of the backbone.

Assuming that the charge density is of three electrons per oligomer of length 10, we should expect carrier concentration of the order of 2.5×10^{21} cm^{-3}. With this concentration at hand, we can convert the simulated mobilities to a conductivity in the order of 12 $S\ cm^{-1}$, a value which is in the range measured for this material.[19]

In our previous studies on one dimensional transport in discotic liquid crystals[20,24,26] relating the transfer integral distribution to mobility was relatively easy: since the transport was one dimensional mobility was essentially set by the tail of low transfer integrals. In three dimensions it is much harder to state *a priori* what will be the rate limiting step when a charge traverses such a box.

One way of doing this is to look at the point when transfer integrals "percolate" the box. Percolation is defined in the following way: we look at clusters of molecules all connected by transfer integrals of at least a certain value J_{min}. We then analyze the size of the largest cluster in the box as a function of J_{min}. Percolation then occurs when J_{min} is large enough to allow charges to traverse the entire box. The percolation threshold is obtained by looking at the relative size of the largest cluster, which is defined as the ratio of number of molecules in the largest cluster to the total number of molecules in a simulation box. This calculation was carried out for the transfer integral between oligomers of length 10. If we allow for a distribution of conjugation lengths to be considered, the interpretation is complicated by the fact that oligomers of different lengths have different aspect ratios and hence different percolation thresholds. The dependence of the relative cluster size on the transfer integral is shown in Fig. 4.

From Fig. 4 it is clear that the value of the transfer integral when the largest interconnected cluster starts spanning the whole box is approximately 10 meV for the slice and isotropic morphologies and slightly over 20 meV for the fiber morphology. This value also corresponds to the first peak in the distribution of intermolecular transfer integrals, peak B, as shown in Fig. 3. In order to convert this limiting transfer integral to a rate for the slowest step we must use the expression from Marcus theory in Eq. (2). In the case when ΔE_{ij} is small and due only to the electric field F, i.e., $\Delta E_{ij} = Fd$, the rate equation for the forward ω_{ij}^{f} and backward ω_{ij}^{b} rates takes the following form:

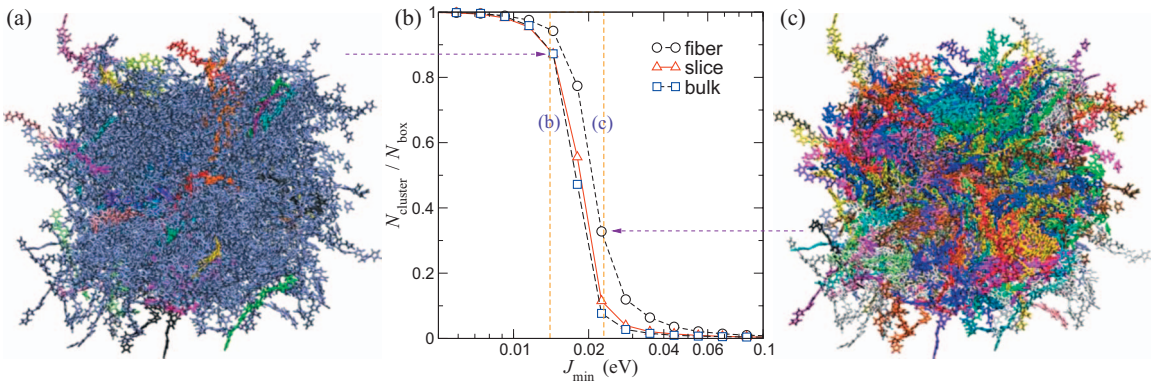

FIG. 4. (a) Simulation snapshot after percolation (J_{min}=23 meV). Different clusters are depicted by different colors. The largest cluster spans the whole box. (b) Relative to the simulation box size of the largest cluster given a certain value J_{min}. (c) Simulation snapshot before percolation (J_{min}=14 meV). Clusters are not well connected and are small compared with the box size.

$$\omega_{ij}^{\mathrm{f,b}} = \frac{J_{ij}^2}{\hbar}\sqrt{\frac{\pi}{k_{\mathrm{B}}T\lambda_{ij}}}\exp\left[-\frac{\lambda_{ij}}{4k_{\mathrm{B}}T}\right]\left(1 \pm \frac{Fd}{2k_{\mathrm{B}}T}\right), \tag{4}$$

where d is the distance between neighboring sites (at the cluster boundary) and all other symbols have the same meaning as in Eq. (2). The mobility can then be calculated as

$$\mu = \frac{d(\omega^{\mathrm{f}} - \omega^{\mathrm{b}})}{F} = \frac{J_{ij}^2 d^2}{\hbar k_{\mathrm{B}}T}\sqrt{\frac{\pi}{k_{\mathrm{B}}T\lambda_{ij}}}\exp\left[-\frac{\lambda_{ij}}{4k_{\mathrm{B}}T}\right]. \tag{5}$$

In other words, we obtain an expression for mobility which is independent of electric field. Notice also that we have assumed that there is no energetic disorder and that all hops are identical. Using $d=5\times10^{-8}$ cm (the first maximum of the radial distribution function), $J_{ij}=0.018$ eV (value which corresponds to the percolation threshold), $k_{\mathrm{B}}T=0.0259$ eV, $\lambda_{ij}=0.35$ eV (average value of the reorganization energy), and $\hbar=6.57\times10^{-16}$ eV s, we obtain an estimate of the mobility of 3×10^{-2} cm^2 V^{-1} s^{-1}. If one looks at Table II it is evident that this estimate of the mobility is indeed a good one.

It is very interesting to note that in fact all the morphologies have rather similar mobilities. In other words it seems that even though the morphologies are very different indeed, the mobilities are all limited by J_{min}, which is similar in all morphologies.

V. CONCLUSIONS

Our main result is that for noncrystalline conjugated polymers charge carrier mobility is insensitive to global orientational molecular ordering. In fact the key morphology parameter as far as mobility is concerned is not so much the regularity of the arrangements of chains, but simply the local packing of the chains which is well represented by the radial distribution function. This is an important observation and debunks an often held opinion that good alignment and orientation of chains is important in order to improve the mobility of a conjugated polymer, at least in the limit of relatively high disorder.

It is also important to emphasize that the proposed model (as any model) makes several approximations. The main ones are (i) the introduction of a concept of a conjugated segment based uniquely on the cutoff of the dihedral angle and (ii) static treatment of chains during charge transport. The latter point is partially addressed by estimating an average lifetime of a conjugated segment of length n.

In conclusion, the mixture of quantum and classical levels of description is used to investigate the link between morphology and charge transport in six different disordered assemblies of polymer. The most important structural parameters are shown to be the local density, as described by the radial distribution function. A method to analyze the three dimensional assembly of polymers is discussed and the concept of a threshold transfer integral is introduced.

ACKNOWLEDGMENTS

This work was partially supported by DFG via IRTG program between Germany and Korea, DFG Grant Nos. AN 680/1-1 and SPP1355. J.K. acknowledges the support of EPSRC and HPC of Imperial College. V.R. acknowledges POLYMAT graduate program. J.K. and D.A. acknowledge the Multiscale Materials Modeling Initiative of the Max Planck Society. We are grateful to Gerhard Wegner, Jianjun Wang, Thorsten Vehoff, Karen Johnston, and Björn Baumeier for fruitful discussions and critical reading of the manuscript.

APPENDIX: ADDITIONAL INFORMATION

1. Force-field parameters

For neutral PPy, the procedure to refine the force-field parameters was already described in Ref. 31 and is briefly recapitulated here. The torsion angle θ of the N–C–C–N dihedral in 2,2′-bipyrrole was scanned and the torsion potential was evaluated using B3LYP hybrid density functional and 6-311++G(3df,3pd) basis set. Calculations were performed using GAUSSIAN package.[53] At each scanning step, the dihedral angle θ was fixed at the value of interest while the rest of the structure was optimized.

To obtain the parameters of the dihedral potential from the *ab initio* potential energy, we took the optimized geometries and let them further relax in MD, constraining the dihedral angle with its parameters set to zero. The force-field based potential energy of these relaxed contributions was then subtracted from the potential energy values provided by *ab initio* calculations.

Partial charges were calculated using B3LYP/6-311G(d,p) and CHELPG (Ref. 54) fitting procedure in a chain of 8 repeat units. A Ryckaerd–Belleman type potential was used to fit the potential energy difference

$$V_{\mathrm{rb}} = \sum_{n=0}^{5} C_n \cos^n \theta. \tag{A1}$$

All force-field parameters are given in Table III.

When oxidized, the polymer changes to a quinoid structure and the backbone of the polymer flattens out. To take this into account at the force-field level, we ignored the changes in bond lengths and adjusted only the dihedral potential and partial charges.

To derive the dihedral potential in the oxidized case, a similar procedure as in the neutral case was performed. Assuming a typical doping rate to be 1 charge per 3 repeat units, we used a charged tetramer to perform the scan. The middle dihedral was constrained to the value of interest while the other two were free to relax. When recalculating the energies in MD, the structure from the quantum chemical calculation was taken, where all three dihedrals restrained to the values obtained in the quantum chemical calculation while the remaining degrees of freedom were relaxed. The Ryckaerd–Belleman parameters were obtained from a multidimensional linear fit to the energy difference.

TABLE III. List of force-field parameters for PPy.

Bonds		
Bond	r_0	k
CW-CW	0.144 23	428 441.6
CS-CS	0.142 40	392 459.2
CW-CS	0.136 70	456 892.8
CS-HA	0.108 00	307 105.6
CW-HA	0.108 00	307 105.6
NA-H	0.101 00	363 171.2
CW-NA	0.138 10	357 313.6
Angles		
Angle	ϕ_0	k
CS-CW-NA	106.500	585.760
CW-NA-CW	109.800	585.760
CW-CS-CS	107.300	585.760
CW-CS-HA	125.700	292.880
HA-CS-CS	127.500	292.880
CW-NA-H	125.100	292.880
NA-CW-CW	121.900	527.000
CS-CW-CW	131.600	527.000
NA-CW-HA	121.600	292.880
CS-CW-HA	132.100	292.880
Atomic charges		
PPY end group		
Atom	Neutral	Oxidized
N	−0.219	−0.426
HN	0.277	0.449
C1	−0.165	0.022
H1	0.157	0.185
C2	−0.172	−0.169
H2	0.124	0.171
C3	−0.195	−0.173
H3	0.127	0.173
C4	0.066	0.068
PPY		
Atom	Neutral	Oxidized
N	−0.3	−0.501
HN	0.3	0.383
C1	0.1	0.235
C2	−0.24	−0.185
H2	0.14	0.159
C3	−0.24	−0.185
H3	0.14	0.159
C4	0.1	0.235

Ryckaerd–Belleman dihedrals							
	Angle	C_0	C_1	C_2	C_3	C_4	C_5
Neutral	NA-CW-CW-NA	16.0392	−2.483 22	−25.8586	3.301 61	11.034	−2.183 95
Oxidized	NA-CW-CW-NA	243.6699	−61.1535	−147.8553	154.0901	75.7420	−102.4387

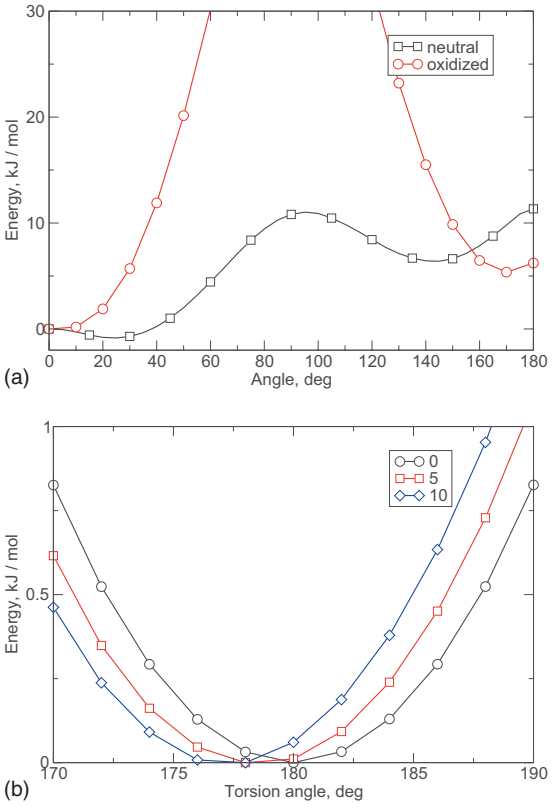

FIG. 5. (a) The torsional barrier of the neutral (black) and the oxidized (blue) polymer. While in the neutral case the equilibrium is approximately 30 and the height of the barrier only a few k_BT, the oxidized state possesses a high barrier and flat geometry. (b) The figure shows the energies when one dihedral angle is fixed at a certain amount while another one is rotated. The calculations show no coupling between the torsion potentials. The curvature stays the same, the small shift can be explained due to nonbonded effects.

To test whether torsional degrees of freedom along the chain are coupled or not, several additional density functional theory scans were performed. In Fig. 5, the scan around an outer dihedral of the tetramer is shown. During this scan, the middle dihedral angle was fixed to 0°, 10°, and 20°. It is clear that the functional form of the potential does not change and only the position of the minimum is affected, which is due to nonbonded interactions.

Furthermore, the potential derived from the tetramer was tested on a hexamer and no significant difference was found. The points described above let us conclude that the same torsional potential can be used for all repeat-unit-linking dihedral angles of the polymer.

2. Lifetime of conjugated segments

An important shortcoming of this model is that it does not consider the fact that the charge transport units are in fact not fixed in time, but change as the torsion angle between conjugated segments fluctuates. These fluctuations occur on time scales of hundred femtoseconds, as can be seen by looking at the distribution of lifetimes for monomers shown in Fig. 6.

The lifetime analysis was performed by doing a short MD run of 40 ps and saving snapshots at each MD step (2 fs). The lifetime was determined by bookkeeping the creation/annihilation of charge units over time due to the variation in torsion angles. The normalized histogram was calculated using 10 fs grid spacing. In the reduced case, only 1.5% of monomers live longer than 5 ps. In the oxidized case, the lifetime of segments of all lengths (except 10-mers) is also shorter than 5 ps.

An important difference of the reduced and oxidized morphologies is the occurrence of conjugated segment lengths. As depicted in Fig. 6(b), the oxidized morphologies consist of mainly conjugated segments of length 10. In the reduced case, short segments are favored.

Because of the short lifetimes, it is important to disregard those simulations where events occur on time scales much slower than this. For example, from Fig. 2 it is evident that if a charge happens by residing on a conjugated segment of length 1 and is surrounded by segments of length greater than 3, the average hopping time will be much longer than the persistence time of that conjugated segment.

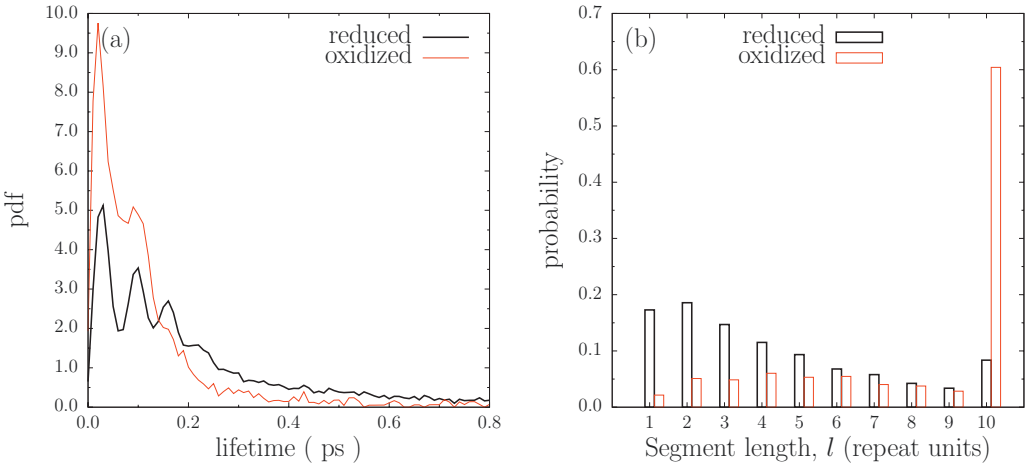

FIG. 6. (a) Lifetime of conjugated segments of length 1. The lifetime of conjugated segments is in the order of couple tenth of picoseconds. (b) Distribution of lengths of conjugated segments. In the reduced case, dimers are the most frequently appearing conjugated segments. In the oxidized case, most of the chains are flat and the most frequent length of a conjugated segment is the total length of an oligomer (10 ru).

[1] A. Murphy and J. Frechet, Chem. Rev. (Washington, D.C.) **107**, 1066 (2007).
[2] J. Roncali, Chem. Rev. (Washington, D.C.) **97**, 173 (1997).
[3] J. Wu, W. Pisula, and K. Müllen, Chem. Rev. (Washington, D.C.) **107**, 718 (2007).
[4] P. Leclère, M. Surin, P. Viville, R. Lazzaroni, A. Kilbinger, O. Henze, W. Feast, M. Cavallini, F. Biscarini, A. Schenning, and E. W. Meijer, Chem. Mater. **16**, 4452 (2004).
[5] P. Leclère, M. Surin, P. Jonkheijm, O. Henze, A. Schenning, F. Biscarini, A. Grimsdale, W. Feast, E. Meijer, K. Müllen, J. L. Brédas, and R. Lazzaroni, Eur. Polym. J. **40**, 885 (2004).
[6] P. Blom and M. Vissenberg, Mater. Sci. Eng. R. **27**, 53 (2000).
[7] R. Kroon, M. Lenes, J. Hummelen, P. Blom, and B. De Boer, Polym. Rev. **48**, 531 (2008).
[8] G. Wegner, Angew. Chem. **20**, 361 (1981).
[9] D. Kumar and R. Sharma, Eur. Polym. J. **34**, 1053 (1998).
[10] A. MacDiarmid, Rev. Mod. Phys. **73**, 701 (2001).
[11] I. McCulloch, M. Heeney, M. Chabinyc, D. DeLongchamp, R. Kline, M. Coelle, W. Duffy, D. Fischer, D. Gundlach, B. Hamadani, R. Hamilton, L. Richter, A. Salleo, M. Shkunov, D. Sparrowe, S. Tierney, and W. Zhang, Adv. Mater. (Weinheim, Ger.) **21**, 1091 (2009).
[12] A. van de Craats, J. Warman, A. Fechtenkotter, J. Brand, M. Harbison, and K. Müllen, Adv. Mater. (Weinheim, Ger.) **11**, 1469 (1999).
[13] H. Sirringhaus, P. Brown, R. Friend, M. Nielsen, K. Bechgaard, B. Langeveld-Voss, A. Spiering, R. Janssen, E. Meijer, P. Herwig, and D. M. de Leeuw, Nature (London) **401**, 685 (1999).
[14] Y. Kim, S. Cook, S. Tuladhar, S. Choulis, J. Nelson, J. Durrant, D. Bradley, M. Giles, I. Mcculloch, C. Ha, and M. Ree, Nature Mater. **5**, 197 (2006).
[15] S. Athanasopoulos, J. Kirkpatrick, D. Martinez, J. Frost, C. Foden, A. Walker, and J. Nelson, Nano Lett. **7**, 1785 (2007).
[16] J. Nelson, J. Kwiatkowski, J. Kirkpatrick, and J. Frost, Acc. Chem. Res. **42**, 1768 (2009).
[17] B. Bolto and D. Weiss, Aust. J. Chem. **16**, 1076 (1963).
[18] K. Lienkamp and G. Wegner, Macromol. Rapid Commun. **28**, 1112 (2007).
[19] A. Diaz, J. Castillo, J. Logan, and W. Lee, J. Electroanal. Chem. **129**, 115 (1981).
[20] J. Kirkpatrick, V. Marcon, J. Nelson, K. Kremer, and D. Andrienko, Phys. Rev. Lett. **98**, 227402 (2007).
[21] D. Andrienko, J. Kirkpatrick, V. Marcon, J. Nelson, and K. Kremer, Phys. Status Solidi B **245**, 830 (2008).
[22] V. Marcon, J. Kirkpatrick, W. Pisula, and D. Andrienko, Phys. Status Solidi B **245**, 820 (2008).
[23] V. Marcon, T. Vehoff, J. Kirkpatrick, C. Jeong, D. Y. Yoon, K. Kremer, and D. Andrienko, J. Chem. Phys. **129**, 094505 (2008).
[24] J. Kirkpatrick, V. Marcon, K. Kremer, J. Nelson, and D. Andrienko, J. Chem. Phys. **129**, 094506 (2008).
[25] V. Marcon, D. Breiby, W. Pisula, J. Dahl, J. Kirkpatrick, S. Patwardhan, F. Grozema, and D. Andrienko, J. Am. Chem. Soc. **131**, 11426 (2009).
[26] X. Feng, V. Marcon, W. Pisula, M. Hansen, J. Kirkpatrick, F. Grozema, D. Andrienko, K. Kremer, and K. Müllen, Nature Mater. **8**, 421 (2009).
[27] A. Lukyanov, C. Lennartz, and D. Andrienko, Phys. Status Solidi A **206**, 2737 (2009).
[28] J. Lopez Cascales, A. Fernandez, and T. Otero, J. Phys. Chem. B **107**, 9339 (2003).
[29] J. J. L. Cascales and T. F. Otero, J. Chem. Phys. **120**, 1951 (2004).
[30] N. McDonald and W. Jorgensen, J. Phys. Chem. B **102**, 8049 (1998).
[31] V. Rühle, J. Kirkpatrick, K. Kremer, and D. Andrienko, Phys. Status Solidi B **245**, 844 (2008).
[32] B. Hess, C. Kutzner, D. van der Spoel, and E. Lindahl, J. Chem. Theory Comput. **4**, 435 (2008).
[33] W. Goedel, G. Holz, G. Wegner, J. Rosenmund, and G. Zotti, Polymer **34**, 4341 (1993).
[34] T. Holstein, Ann. Phys. (N.Y.) **8**, 343 (1959).
[35] A. Romero, D. Brown, and K. Lindenberg, Phys. Lett. A **266**, 414 (2000).
[36] L. Zoppi, A. Calzolari, A. Ruini, A. Ferretti, and M. Caldas, Phys. Rev. B **78**, 165204 (2008).
[37] D. Cheung, D. McMahon, and A. Troisi, J. Phys. Chem. B **113**, 9393 (2009).
[38] A. Troisi and G. Orlandi, Phys. Rev. Lett. **96**, 086601 (2006).
[39] A. Troisi, D. Cheung, and D. Andrienko, Phys. Rev. Lett. **102**, 116602 (2009).
[40] K. F. Freed and J. Jortner, J. Chem. Phys. **52**, 6272 (1970).
[41] R. A. Marcus, Rev. Mod. Phys. **65**, 599 (1993).
[42] R. Singh and A. Narule, Synth. Met. **82**, 245 (1996).
[43] P. Barbara, T. Meyer, and M. Ratner, J. Phys. Chem. **100**, 13148 (1996).
[44] J. Kirkpatrick, Int. J. Quantum Chem. **108**, 51 (2007).
[45] J. L. Brédas, B. Themans, and J. M. Andre, Phys. Rev. B **27**, 7827 (1983).
[46] J. L. Brédas, J. C. Scott, K. Yakushi, and G. B. Street, Phys. Rev. B **30**, 1023 (1984).
[47] J. L. Brédas, B. Themans, J. G. Fripiat, J. M. Andre, and R. R. Chance, Phys. Rev. B **29**, 6761 (1984).
[48] R. R. Chance, J. L. Bredas, and R. Silbey, Phys. Rev. B **29**, 4491 (1984).
[49] R. Colle and A. Curioni, J. Am. Chem. Soc. **120**, 4832 (1998).
[50] R. Colle and A. Curioni, J. Phys. Chem. A **104**, 8546 (2000).
[51] J. Nelson and R. Chandler, Coord. Chem. Rev. **248**, 1181 (2004).
[52] V. Rühle, C. Junghans, A. Lukyanov, K. Kremer, and D. Andrienko, J. Chem. Theory Comput. **5**, 3211 (2009).
[53] M. J. Frisch, G. W. Trucks, H. B. Schlegel *et al.*, GAUSSIAN03, Revision C.02, Gaussian, Inc., Wallingford, CT, 2004.
[54] C. B. Breneman and K. E. Wiberg, J. Comput. Chem. **11**, 361 (1990).